Available online at www.sciencedirect.com
ScienceDirect
Journal of Nuclear Materials 375 (2008) 185–191
journal of nuclear materials
www.elsevier.com/locate/jnucmat

Void swelling in a 9Cr ferritic/martensitic steel irradiated with energetic Ne-ions at elevated temperatures

C.H. Zhang [a,b], J. Jang [a,*], M.C. Kim [a], H.D. Cho [a], Y.T. Yang [b], Y.M. Sun [b]

[a] *Korea Atomic Energy Research Institute, Nuclear Material Technology Developments Division, 150, Deokjin-dong, Yuseong-gu, Daejeon 305-353, South Korea*

[b] *Institute of Modern Physics, Chinese Academy of Sciences, Lanzhou 730000, PR China*

Received 3 October 2006; accepted 5 November 2007

Abstract

In this work the void swelling behavior of a 9Cr ferritic/martensitic steel irradiated with energetic Ne-ions is studied. Specimens of Grade 92 steel (a 9%Cr ferritic/martensitic steel) were subjected to an irradiation of ^{20}Ne-ions (with 122 MeV) to successively increasing damage levels of 1, 5 and 10 dpa at a damage peak at 440 and 570 °C, respectively. And another specimen was irradiated at a temperature ramp condition (high flux condition) with the temperature increasing from 440 up to 630 °C during the irradiation. Cross-sectional microstructures were investigated with a transmission electron microscopy (TEM). A high concentration of cavities was observed in the peak damage region in the Grade 92 steel irradiated to 5 dpa, and higher doses. The concentration and mean size of the cavities showed a strong dependence on the dose and irradiation temperature. Enhanced growth of the cavities at the grain boundaries, especially at the grain boundary junctions, was observed. The void swelling behavior in similar 9Cr steels irradiated at different conditions are discussed by using a classic void formation theory.

PACS: 61.80.Jh

1. Introduction

Ferritic/martensitic steels are being considered as candidate materials for the structural components in the Generation IV or the fusion DEMO reactors, due to their several attractive merits such as low activation, resistance to a void swelling, low thermal expansion coefficients and high thermal conductivity. The response of these materials to an intensive irradiation of energetic particles (especially neutrons which cause a displacement damage and the production of some gaseous impurities like helium) is an important issue for the use of these materials in an advanced nuclear power plant [1]. Previous work on the response of such materials to an energetic particle irradiation focused on a low temperature range (below 300 °C) where the irradiation hardening and flow localization in the presence of helium is an important concern [2–6]. However, defect production and helium effects at higher temperatures have not been fully explored [1,7]. It is expected that at temperatures above $0.3T_m$ a helium accumulation may cause severe embrittlement at the grain boundaries and an enhancement of the void swelling of metallic alloys at high displacement damage levels [8].

On the other hand, an irradiation with energetic ions has been used as a screening test method to evaluate the irradiation response of candidate materials, or has been used to study some fundamental aspects of an irradiation damage like cascade damage structures or helium effects. In the present work, microstructural changes of a 9Cr ferritic/martensitic steel irradiated with high-energy Ne-ions as a function of the irradiation dose and temperature were studied. Since Ne atoms have been proven to have a similar behavior to helium in irradiated metals [9], high-energy

* Corresponding author.
E-mail address: jjang@kaeri.re.kr (J. Jang).

0022-3115/$ - see front matter © 2008 Elsevier B.V. All rights reserved.
doi:10.1016/j.jnucmat.2007.11.009

Ne-ions were used in the present study to introduce, on the one hand, a high displacement damage (at a higher damage rate than usually helium ions do), and on the other hand, neon-gas atoms to simulate the helium effects.

2. Experimental

The material used in the present irradiation is a 9Cr ferritic/martensitic steel (Grade 92 steel), which was hot rolled, normalized at 1060 °C and tempered at 780 °C. The composition of the alloy is given in Table 1. One surface of each specimen with a size of $13 \times 6 \times 0.3$ mm^3 was mechanically ground with down to 0.3 mm alumina powders, and then electrolytically polished in a solution of 1000 ml of acetic acid and 70 ml of perchloric acid with the voltage of 20 V for 30 s.

The irradiation was performed in a terminal chamber (in a vacuum of about 2×10^{-4} Pa) of the separate fan cyclotron (SFC) in the National Laboratory of Heavy-ion Accelerators in Lanzhou, China. $^{20}Ne^{7+}$ ions with a kinetic energy of 122 MeV were used for the irradiation. The ion beam was raster scanned using two sets of magnets installed at the front beam line, with scanning frequencies of 73.5 Hz in the horizontal direction and 37 Hz in the vertical direction. The scanned beam size was 25×25 mm^2. An aperture with a diameter of 11 mm was amounted in front of the specimens to limit it to an area of ∅12 mm for a uniform irradiation. A Grade 92 steel specimen and a MA956 alloy (a 20Cr ferritic oxide dispersion strengthened alloy) specimen were irradiated simultaneously. The results of the MA956 alloy specimens are going to be presented in a separate paper. Specimens of the Grade 92 steel were irradiated with Ne-ions to three successively increasing fluences of 6.25×10^{15}, 3.13×10^{16}, and 6.25×10^{16} ions/cm^2 (which correspond to the estimated displacement levels of 1, 5 and 10 dpa, respectively, at a damage peak according to the SRIM96 code [10]) at 440 °C, and for two fluences of 3.13×10^{16}, and 6.25×10^{16} ions/cm^2 at 570 °C. In these conditions the intensity of the ion beam was purposely controlled to minimize the beam-heating effect. The dose rate was about 0.5 dpa/h at a damage peak with a fluctuation within ±25%.

The temperatures were stable over most of the irradiation time with a fluctuation within ±15 °C. Beside the above 'constant temperature' conditions, an irradiation during a 'temperature ramp' was performed with the temperature increasing from 440 to 630 °C. The temperature was increased rapidly from 440 to 590 °C at a rate 7.8 °C /min, and increased slowly from 590 to 640 °C at a rate of 0.07 °C /min.

Table 1
Chemical composition of the Grade 92 F/M steel specimens (wt%)

Fe	C	Si	Mn	Cr	Ni	Mo	V	W	Al
Bal.	0.11	0.18	0.43	8.91	0.12	0.47	0.19	1.67	0.004

Table 2
Details of irradiation experimental condition (with a Ne/dpa ratio of 1200 appm/dpa)

Irradiation Temperature (°C)	Ion fluence (ions/cm^2)	dpa at max.	C_{Ne} at max. (at.%)
440	6.25×10^{15}	1	0.12
570	3.13×10^{16}	5	0.60
	6.25×10^{16}	10	1.2

At the temperature of 570 °C, only the intermediate (5 dpa) and high dose (10 dpa) irradiation were done.

During an irradiation the temperature was measured by using a thermal couple mounted at a corner of the specimen (outside of the irradiated area). A calibration experiment using a blank specimen was also performed prior to the former irradiations to correct the difference of the temperature between the periphery of the irradiated area (about 12 mm in diameter) and the corner of the irradiated area, using two thermal couples which were also shielded from a direct beam-heating. The main parameters for the irradiation experiment are summarized in Table 2. The Ne/dpa ratio at a damage peak was about 1200 appm/dpa, which is higher than the He/dpa ratios in a fusion reactor (10–15 appm/dpa in metallic alloys) and in a fast reactor (0.1 appm/dpa) [1].

After an irradiation, each specimen was nickel-coated to a thickness of about 3 mm by an electroplating technique in a solution of $NiCl_2$ and $NiSO_4$ (at a ratio of 1:2). The Ni-coated specimens were cut into cross-sectional samples using a low-speed diamond cutter. Discs with 3 mm in diameter were cut from two cross-sectional slices of each irradiated specimen by using a South Bay Technology slurry cutter. The irradiated area in the cross-sectional slices was further thinned by using a dimple grinder and a Precision Ion Polishing System (Gatan 691, with two Ar ion beams of 5 keV, incident at the glancing angles around 4° to the specimen surface). The TEM samples were investigated in a JEOL FX2000 which was operated at 200 kV.

3. Results

A typical TEM micrograph of a cross-sectional specimen is shown in Fig. 1. Contrast of the peak damage region at a depth of about 31 μm beneath the specimen surface is obvious when irradiated to 5 dpa or to higher damage levels. This depth is close to the value (32 μm) estimated by the Monte Carlo code SRIM96 [10]. No cavities were observed in the peak damage region irradiated to 1 dpa at 440 °C. However, cavities were observed in the specimens irradiated to 5 or 10 dpa at 400 and 570 °C, and also in the specimens irradiated in the ramp temperature condition. It is thus found that the dose threshold for a cavity formation during a Ne-ion irradiation is between 1 and 5 dpa.

Typical microstructures of the cavities in the peak damage regions of the irradiated specimens under the constant

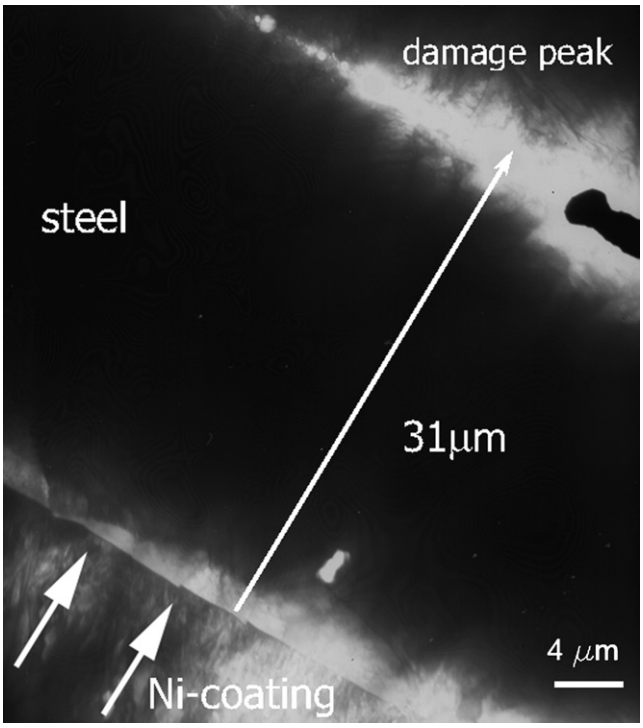

Fig. 1. A TEM micrograph at a low magnitude of a cross-sectional specimen, irradiated at 440 °C to a peak damage of 10 dpa.

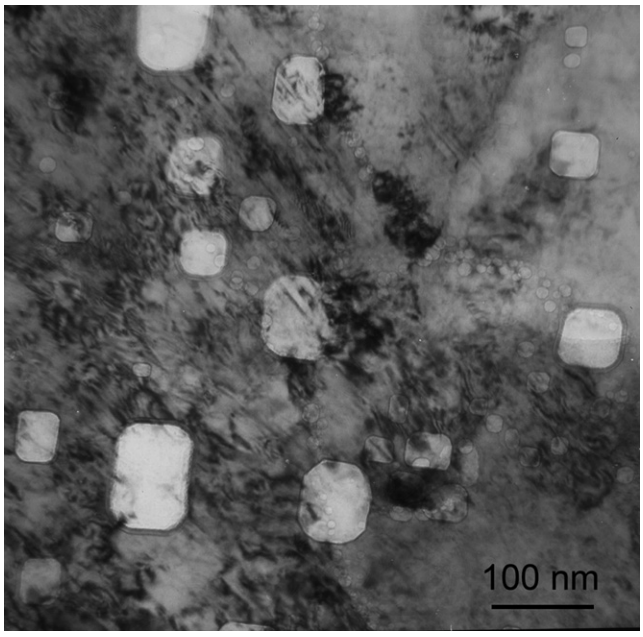

Fig. 3. Typical microstructures of the cavities in the peak damage regions of the specimen irradiated under the temperature ramp condition.

temperature conditions are shown in Fig. 2. And the microstructure of the cavities in the temperature ramp condition alone is shown in Fig. 3. In some conditions (within a martensite lath, shallower depth regions) the cavities tend to be a facet-shape, with their faces at some low-index planes like (1 0 0), (1 1 0), (1 1 2), (1 2 3), etc. It is evident that the cavity structure has a strong dependence on the irradiation dose and temperature. Significant increase of the cavity size with an increase of the dose and irradiation temperature is apparent. A typical size distribution of the cavities is found to be composed of a narrow peak at a smaller size range and a broad peak (or tail) at a larger size range, as shown in Fig. 4. Such a size distribution provides evidence of a possible coarsening mechanism of the cavities via a dislocation-bias-driven growth [11].

The number density, average effective diameter of the cavities and the calculated void swelling in the peak damage regions for the irradiated specimens are given in Fig. 5, where the number density of the cavities was obtained using the thickness data of the specimen in the cavity region obtained by the K-M pattern from the CBED method, as described in detail in Ref. [12]. The mean effective diameter of the cavities increases with an increasing irradiation dose and temperature while the number density tends to saturate above 5 dpa, thus the calculated void

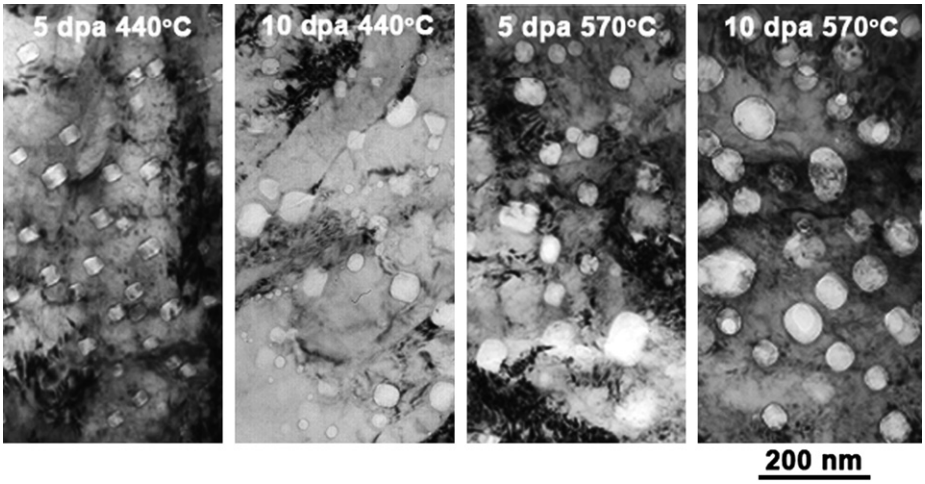

Fig. 2. Typical microstructures of the cavities in the peak damage regions of the specimens irradiated at different conditions. Bright field kinematically under-focused images.

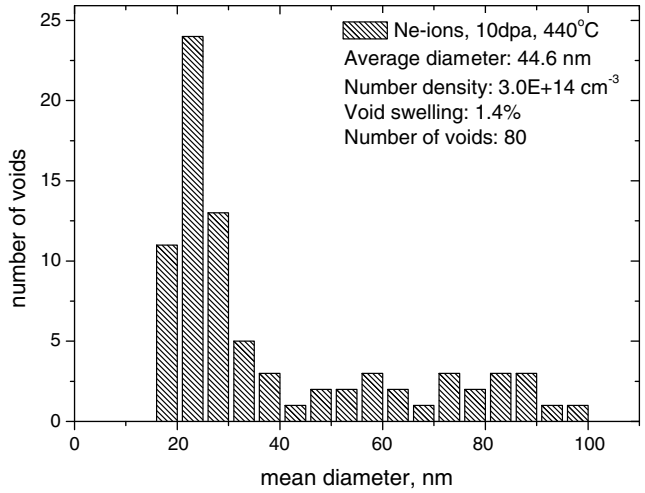

Fig. 4. Typical size distribution of the cavities in the specimen irradiated at 440 °C to a peak damage of 10 dpa.

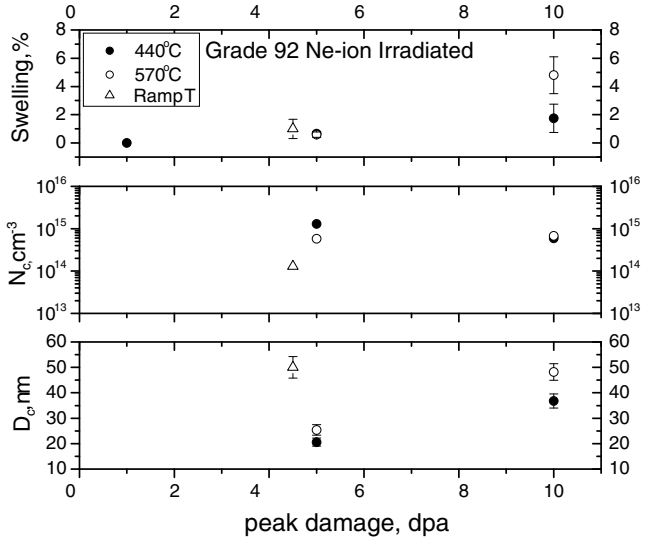

Fig. 5. Number density and average effective diameter of the cavities, and the calculated void swelling in the peak damage regions of the irradiated specimens.

swelling increases with the increasing dose. There is a minor difference in the void swelling at 5 dpa between the irradiations at 440 and 570 °C, while at a higher dose of 10 dpa the void swelling is significantly greater at 570 than at 440 °C. The maximum void swelling (4.8%) occurred in the specimen irradiated to 10 dpa at 570 °C. And the maximum mean diameter (~50 nm) was found in the temperature ramp condition (at 4.5 dpa). Since the specimen reached the highest temperature, 630 °C in the temperature ramp condition among the present irradiation conditions, the high temperature is assumed to be the main reason for the enhanced growth of the cavities.

Another important feature of the cavities in the irradiated specimens is the preferential nucleation of the cavities at the prior-austenitic grain boundaries and the lath boundaries. Typical microstructures at the prior-austenitic grain boundaries and at the lath boundaries were shown in Fig. 6(a) and (b), respectively. Enhanced growth of the voids occurred especially at the triple junctions, while no enhanced growth of the cavities was observed at the lath boundaries. In the peak damage region with an increasing number density, the cavities tend to form more homogenously in the matrix.

In addition, the TEM investigation found no preferential formation of the cavities at the interfaces of the needle-shaped carbides, which are distributed in the martensite lath, as shown in Fig. 7. It is found that the interfaces of the needle-shaped carbides in the martensite lath do not provide favorable sites for a cavity nucleation,

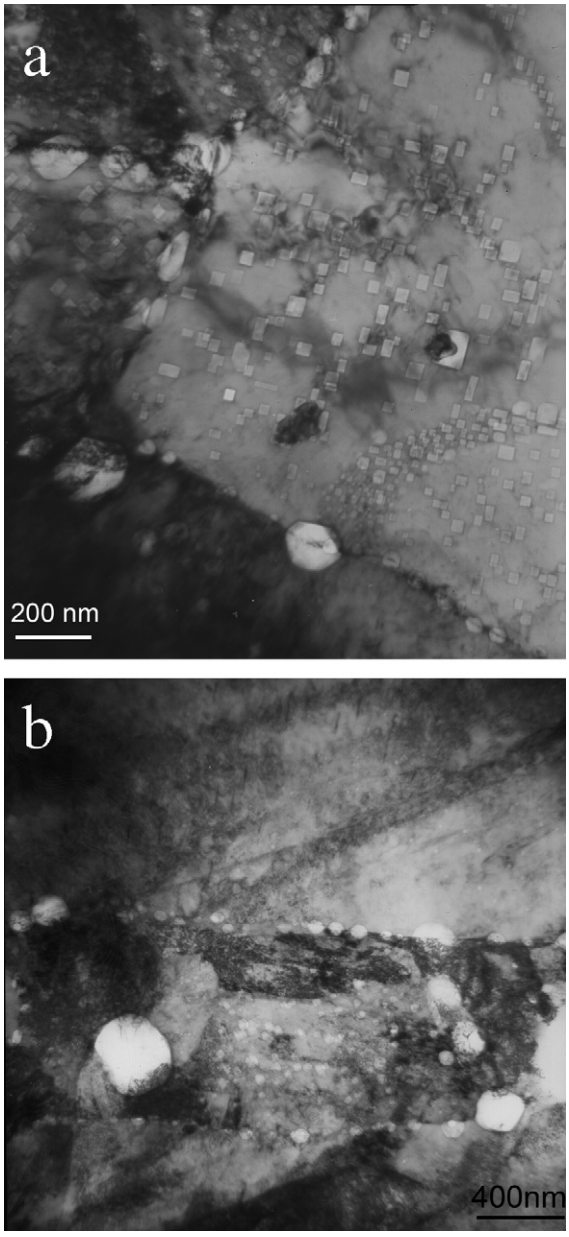

Fig. 6. (a) Enhanced nucleation and growth of the cavities at the prior-austenite grain boundaries, (b) enhanced nucleation of the cavities at the lath boundaries. The specimen was irradiated at 440 °C to a peak damage of 10 dpa.

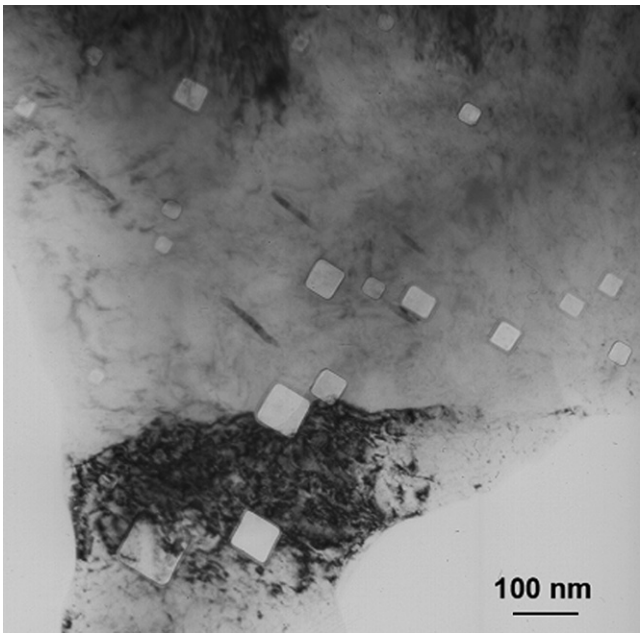

Fig. 7. Cavities with needle-shaped carbides in the martensite lath in the specimen irradiated at 570 °C to a peak damage of 5 dpa.

as the prior-austenitic grain boundaries and the lath boundaries did.

4. Discussion

In this section we try to establish a correlation of the data of the cavity formation and the void swelling in 9Cr ferritic/martensitic steels irradiated with different particles (He-ions, Ne-ions, Fe/He dual-ions, self-ions, and fast neutrons). Even though irradiations with particles (He, Ne, self-ions, dual beams, fast neutrons) produce similar trends of the irradiation effects (defect production, void swelling, mechanical property changes, etc.), there are significant differences in the dose threshold for a cavity formation, cavity density and size, swelling rate, etc. It is therefore important to understand the difference in a cavity formation and a void swelling under different irradiation conditions.

In the present study the correlation of the data for cavities from different experiments is discussed using the gas concentration to dpa ratio as a key factor. Helium atoms were found to stabilize vacancy clusters and enhance a cavity formation [11]. Similar effect of a stabilization of vacancy clusters by oxygen atoms (mainly through a chemical bonding with the atoms at an interface) was also found [13]. There is a large difference in the gas concentration to dpa ratios in different irradiation conditions (ranging from 10^4 appm/dpa in the case of a He-ion irradiation to 10^{-2} appm/dpa in the case of a Ni-ion irradiation). Here we used a model based on a diffusion-controlled helium bubble formation using a rate equation approach to describe the dynamics of the main defect species (i, v, i-loops, He/v clusters, cavities) during irradiation [14,15]. The main points of the model are described as follows.

The concentration evolution for four kinds of 'point defects' including self-interstitials, vacancies, helium atoms in an interstitial site, helium atoms in a substitutional site are described separately using a set of coupled rate equations. The 'dissociative mechanism' (including the thermal dissociation mechanism, and the self-interstitial/He replacement mechanism [14,16]) was incorporated to describe the transition of substitutional He to interstitial He.

Bubble formation is described by using the di-atomic nucleation model, where two helium atoms are assumed to compose a stable nucleus [14]. The shrinkage/growth of the bubbles is assumed to depend on an ejection/trapping of the self-interstitials, vacancies or interstitial helium atoms. The 'loop-punching' mechanism [17] is also included to describe the growth of bubbles when the inner pressure exceeds the limit of a mechanical instability. Bubble formation at the dislocations is also included from the following literature [18]. The formation of self-interstitial loops and the growth of dislocations are considered. Bubble growth via a migration and coalescence (M&C) [19] mechanism was not included. And the possible effects of grain boundaries on a bubble formation were not considered.

The present model was implemented based on our previous theoretical work as given in our previous paper [20]. The model was used to interpret the temperature dependence of the cavities in helium-implanted stainless steels using the rate equation approach. In the present model we introduced the concept of the critical size for the bias-driven growth [11,21] (i.e. a critical number of helium atoms are required in a cavity to achieve a continuous growth during an irradiation) to distinguish the voids (cavities above the critical size) from the small helium bubbles. Consequently, the rate equations were also expanded, by using each rate equation to describe the bubbles containing a given number of helium atoms (below the critical size). The average size and number density of the voids are described with another two rate equations. An average density of the dislocations of 10^{12} cm^{-2} was used in the calculation. A number density of 10^{12} cm^{-3} was used as the criterion for an observable cavity population. The calculation was done corresponding to an irradiation temperature of 800 K. The main parameters (for example the diffusion coefficient of different point defects, and a recombination or trapping radius, etc.) in our previous work [20] were used.

The dependence of the number density of the voids on the irradiation dose from the calculation is given in Fig. 8, corresponding to different He-to-dpa ratios. We found that the number density and size of the voids (cavities containing helium atoms more than the critical number for continuous bias-driven growth) depended strongly on the He-to-dpa ratio, the pre-irradiation dislocation density, and the dose rate, while they were less dependent on some intrinsic factors like the effective diffusion coefficient and the trapping radius. At the high He-to-dpa ratios the

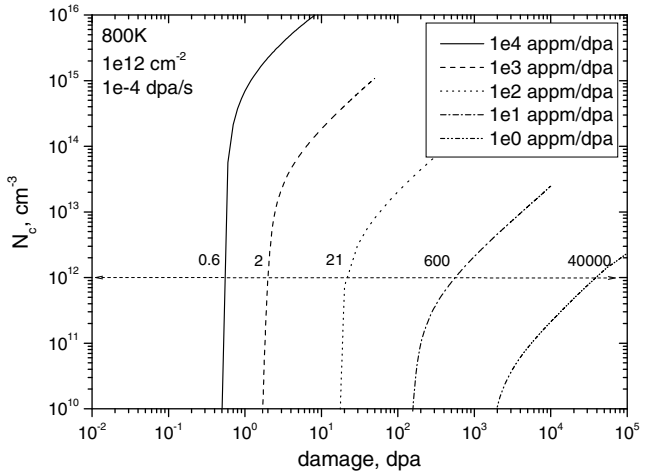

Fig. 8. Dose dependence of the number densities of the voids formed under different He-to-dpa ratios from the theoretical calculation. The horizontal dashed line shows the observable limit of the void number density in TEM.

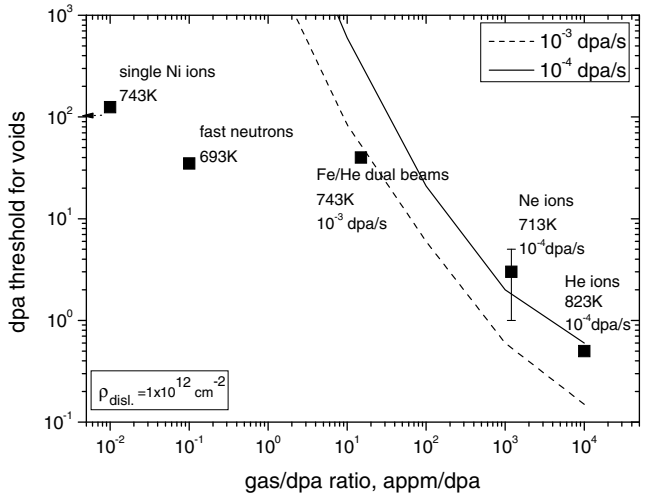

Fig. 9. The dose threshold for a cavity formation in 8–9Cr ferritic/martensitic steels at temperatures around 800 K as a function of the gas concentration to dpa ratio, the experimental data (in symbols) and the theoretical estimates (in lines corresponding to the two dose rates) are given.

calculation showed that there are definite dose thresholds for an observable void population.

The dose threshold for a void formation as a function of the gas concentration to dpa ratio is shown in Fig. 9, where the theoretical estimates are given as lines corresponding to two different damage rates (10^{-4} and 10^{-3} dpa/s). Experimental data from the irradiations of 9Cr F/M steels with He-ions [5], dual-ions and Ni-ions [22], fast neutrons [23], and the present Ne-ions (the error bar shows the range of uncertainty between 1 and 5 dpa), performed at temperatures between 700 and 850 K, are also compiled and plotted in the figure. The data are plotted as a function of the inert-gas concentration to dpa ratios in the given conditions except for the Ni-ion irradiation. In the case of the Ni-ion irradiation the O to dpa ratio is used. The residual oxygen concentration is expected to be around 1 appm, and the O to dpa ratio is estimated to be around 0.01 appm/dpa. The dose threshold for the Ni-ion irradiation varies for different experiments from about 120 dpa [22] to 250 dpa [24], possibly due to a difference in the residual O concentration.

From Fig. 9 a good correlation between the theoretical and measured dose thresholds for a void formation in the 9Cr F/M steels irradiated with He-ion, Ne-ion and Fe/He dual ion beams is found at over three orders of a magnitude of the inert-gas concentration/dpa ratio based on the model, indicating that the large difference in the damage threshold for a void formation is understandable with the inert-gas concentration/dpa ratio as the key factor. As the gas concentration/dpa ratios drop below 10 appm/dpa, the experimental data suggests a saturation behavior, which is not predicted by the model. We think that the saturation manner of the dose threshold at low He-to-dpa ratios may be attributed to the role of the grain boundaries during a cavity nucleation, which was not included in the model. The much lower dose threshold of the fast neutron irradiation may also suggest the possible role of cascade damage during a void formation, possibly through the proposed in-cascade nucleation or the cascade damage impeded diffusion [25]. Also the proposed migration and coalescence (M&C) [17] of small bubbles is expected to enhance a void formation in the case of a fast neutron irradiation where the dose rate is the lowest among the irradiation conditions.

In addition to the dose thresholds, we also compiled data on the swelling rate (void swelling per dpa) from different experiments as a function of the gas concentration to dpa ratio, as shown in Fig. 10, where the error range for the swelling data was estimated as 50%. It is interesting to find that the data for the swelling rate under various irradiation conditions follows a simple function of the gas concentration to dpa ratio:

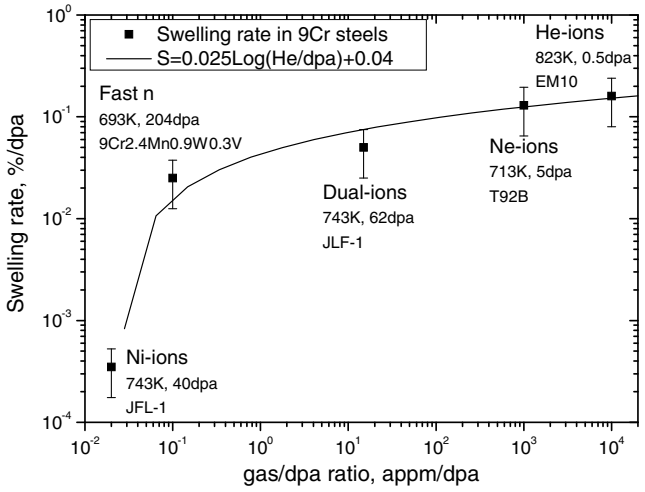

Fig. 10. The swelling rate (void swelling per dpa) from different irradiation experiments as a function of the gas concentration to dpa ratio.

$$S = 0.025\mathrm{Log}_{10}(\mathrm{He/dpa\ ratio}) + 0.04, \quad (1)$$

where S is the swelling rate in % per dpa, and the He/dpa ratio in appm/dpa. Neither the number density nor the average effective diameter of the cavities was found to follow a simple function. This result suggests an important role of the gas concentration to dpa ratio during a void swelling. Physical mechanisms for the correlation of the void swelling data from different experiments need further study.

5. Conclusion

In the Grade 92 steel (a 9Cr F/M steel) specimens irradiated with high-energy Ne-ions, a dose threshold between 1 and 5 dpa for a cavity formation was found. The cavity structure was found to strongly depend on the irradiation dose and temperature. The maximum size of the voids was found in the temperature ramp condition where the temperature reached 630 °C, while the maximum void swelling (4.8%) occurred for an irradiation to 10 dpa at 570 °C. Enhanced nucleation of the cavities at the prior-austenitic grain boundaries and the lath boundaries was found. Also an enhanced growth of cavities at grain boundary junctions was observed.

Data on a cavity formation in 9Cr F/M steels from different irradiation conditions was compiled and discussed using a classical void formation theory. Good correlation of the dose threshold for a void formation in the cases of He-ion, Ne-ion and Fe/He dual ion irradiations was found using the inert-gas concentration to dpa ratio as a key factor, indicating that the large difference in the dose threshold for a void formation is understandable on the basis of the applied classical theory for a void formation. The swelling rates for different irradiation conditions were also found to follow a simple function of the gas concentration to dpa ratio.

Acknowledgments

One of us (CHZ) would like to thank the Brain Pool Program of Korean Federation of Science and Technology (KOFST) for the support of his visit to Korean Atomic Energy Research Institute. We also thank Dr Y.F. Jin, Z.G. Wang and other colleagues for their help in the irradiation experiment, and to V&M Tubes, France for the kind provision of Grade 92 steel samples.

References

[1] L.K. Mansur, A.F. Rowcliffe, R.K. Nanstad, S.J. Zinkle, W.R. Corwin, R.E. Stoller, J. Nucl. Mater. 329–333 (2004) 166.
[2] Y. Dai, X.J. Jia, K. Farrell, J. Nucl. Mater. 318 (2003) 192.
[3] X. Jia, Y. Dai, J. Nucl. Mater. 323 (2003) 360.
[4] P. Jung, J. Henry, J. Chen, J.C. Brachet, J. Nucl. Mater. 318 (2003) 241.
[5] J. Henry, M.H. Mathon, P. Jung, J. Nucl. Mater. 318 (2003) 249.
[6] Y. Katoh, H. Tanigawa, T. Muroga, T. Iwai, A. Kohyama, J. Nucl. Mater. 271&272 (1999) 115.
[7] S.A. Maloy, J. Nucl. Mater. 343 (2005) 367.
[8] H. Ullmaier, Radiat. Eff. 78 (1983) 1.
[9] N. Marochov, P.J. Goodhew, J. Nucl. Mater. 158 (1988) 81.
[10] J.F. Ziegler, J.P. Biersack, U. Littmark, The Stopping and Range of Ions in Solids, vol. 1, Pergamon, New York, 1984.
[11] L.K. Mansur, W.A. Coghlan, J. Nucl. Mater. 119 (1983) 1.
[12] D.B. Williams, C.B. Carter, Transmission Electron Microscopy, Plenum, New York and London, 1996, p. 321.
[13] S.J. Zinkle, E.H. Lee, Metall. Trans. A 21 (1990) 1037.
[14] H. Trinkaus, J. Nucl. Mater. 118 (1983) 39.
[15] M. Fell, S.M. Murphy, J. Nucl. Mater. 172 (1990) 1.
[16] N.M. Ghoniem, S. Sharafat, J.M. Williams, L.K. Mansur, J. Nucl. Mater. 117 (1983) 96.
[17] W.G. Wolfer, Philos. Mag. A 58 (1988) 285.
[18] B.N. Singh, T. Leffers, W.V. Green, M. Victoria, J. Nucl. Mater. 125 (1984) 287.
[19] R.S. Barnes, D.J. Mazey, Proc. Royal Soc. London, A 275 (1963) 47.
[20] C.H. Zhang, K.Q. Chen, Z.Y. Zhu, Nucl. Instrum. and Meth. B 169 (2000) 64.
[21] E.H. Lee, L.K. Mansur, Metall. Trans. A 21 (1990) 1021.
[22] H. Ogiwara, H. Sakasegawa, H. Tanigawa, M. Ando, Y. Katoh, A. Kohyama, J. Nucl. Mater. 307–311 (2002) 299.
[23] (a) D.S. Gelles, J. Nucl. Mater. 212–215 (1994) 714;
(b) A. Kimura, H. Matsui, J. Nucl. Mater. 212–215 (1994) 701;
(c) Y. Kohno, A. Kohyama, M. Yoshino, K. Asakura, J. Nucl. Mater. 212–215 (1994) 707.
[24] J. Gan, T.R. Allen, J.I. Cole, S. Ukai, S. Shutthanandan, S. Thevuthasan, Mater. Res. Symp. Proc. 792 (2004) 13.
[25] H. Trinkaus, B.N. Singh, A.J.E. Foreman, J. Nucl. Mater. 174 (1990) 80.